Full Paper

Mechanistic Insights on the Formation of high-valent $Mn^{III/IV}$=O Species Using Oxygen as Oxidant: A Theoretical Perspective

Asmita Sen[+],[a] Nidhi Vyas[+],*[a, b] Bhawana Pandey,[a] Madhavan Jaccob,[a, c] and Gopalan Rajaraman*[a]

Abstract: High-valent metal–oxo species are of great interest as they serve as a robust catalyst for various organic transformations, and at the same time, they offer significant insight into the reactivity of various metalloenzymes. Formation of Mn–Oxo species is of great interest as they are involved in the Oxygen Evolving Complex of Photosystem II, and various bio-mimic models were synthesized to understand its reactivity. In this context, using urea decorated amine ligands, Borovik et al. have reported the facile formation of Mn^{III}=O and Mn^{IV}=O species from $[Mn^{II}H_2buea]^{2-}$ (here H2buea = tris[(N'-$tert$-butylureayl)-N-ethyl] amine) precursor complex using oxygen as the oxidant. While reactivity of these species is thoroughly studied, mechanism of formation of such species is scarcely explored. In this work, we have attempted to establish the formation of these species from the Mn^{II} precursor using the experimental conditions. Our calculations reveal the following fundamental steps in the formation of such species: i) O_2 activation by Mn^{II} lead to formation of Mn^{II}–superoxide species wherein the oxidation state of the Mn^{II} found to be intact upon O_2 binding facilitated by the deprotonated nitrogen atom present in the cavity (ii) in the second step, superoxo species is converted to Mn^{II}–hydroperoxo species, $[Mn^{II}H_2buea(OOH)]^{2-}$ using dimethylacetamide solvent as source for HAT reaction (iii) presence of water molecule found to aid the O–O bond cleavage in $[Mn^{II}H_2buea(OOH)]^{2-}$ species leading to the formation of the putative Mn^{III}=O species, $[Mn^{III}H_3buea(O)]^{2-}$ (iv) one-electron oxidation of Mn^{III}=O, leads to the formation of $[Mn^{IV}H_3buea(O)]^-$ species and this step is endothermic and need some external oxidants for its formation. While various spin-states and their roles are explored, our calculations reveal that the Mn atom prefers to be in the high-spin state across the potential energy surface studied. However, the nature of the formation is strongly correlated to the spin state arising from the radical nature present in the O_2 moiety and also in the deprotonated nitrogen atom. This offers a unique multistate reactivity channel for the formation these species easing various kinetic barriers across the potential energy surface. Further, we have also computed the spectral parameters for the experimentally observed species, which are in agreement with the reported data offering confidence on the mechanism established. To this end, our study unveils a facile formation of high-valent Mn–Oxo species using O_2 as oxidant and role of water molecules in the formation of such species, and these mechanistic insights are likely to have implications beyond the example studied here.

Keywords: high-valent Mn–oxo · Mn^{III}=O · Mn^{IV}=O · H_3buea · metalloenzyme

1. Introduction

Over the past decades, much attention has been paid to the study of the high-valent metal–oxo species with manganese and iron metals in particular because they are well known as a key intermediate in a variety of oxygenation reactions by metalloenzymes and metal catalysts.[1,2] These metalloenzymes have paved the way for biomimetic studies as they can solve the mystery behind the complexity of the biochemical processes, and this knowledge will help in designing new catalysts with high efficiency and more selectivity of pharmaceutical interest. Numerous metal–oxo complexes have been synthesised and characterised by spectroscopy, which is involved in C–H bond activation as well as oxygen atom transfer reactions.[3] Several studies on the catalytic potential of biomimetic iron–oxo complexes towards the C–H bond activation were explored dramatically to ensure a clear under-

standing of the important geometrical, functional, and mechanistic features of the corresponding enzyme counterparts.[4] According to the literature, Mn–O species have also attracted

[a] *A. Sen,[+] N. Vyas,[+] B. Pandey, M. Jaccob, G. Rajaraman*
Department of Chemistry, Indian Institute of Technology Bombay, Mumbai 400076, India
E-mail: nidhivyas12@gmail.com
rajaraman@chem.iitb.ac.in

[b] *N. Vyas[+]*
School of Biotechnology, Jawaharlal Nehru University, New Delhi - 110067, India

[c] *M. Jaccob*
Department of chemistry, Loyola College, Chennai – 600 034.

[+] *both authors contributed equally.*

Supporting information for this article is available on the WWW under https://doi.org/10.1002/ijch.201900142

much attention as an important intermediate in a wide range of catalytic reactions such as; photosystem II,[5] peroxidases,[6] and catalases.[7] However, the synthetic manganese–oxo complexes, such as those with imines and porphyrin ligands, have been postulated to be reactive species in catalytic oxidations of various compounds. The formation of terminal Mn/Fe–O complexes is facilitated by the high oxidation states (generally $\geq 4+$) of the corresponding metal so that they can form multiple bonds with the oxo-group, which eventually stabilise the M–O moiety. In contrast, manganese complexes in their low-vacancies, such as $3+$ valence with the terminal oxo ligands in the axial position, are scarce because these low-valent complexes tend to dimerise and form species like μ-oxo bridged Mn(III)–(O)$_n$–Mn(III) dimers (n = 1–3).[9] Therefore, it is important to understand the factors which can stabilise the terminal Mn–O complexes in the $+3/+4$ oxidation states as these are highly relevant for the active site structure of OEC of photosystem II. In the metalloproteins the terminal oxo species are generally stabilised by intramolecular hydrogen bonding interactions from the active site residues and this type of intramolecular interaction between the oxo and the properly placed hydrogen bond donors in the cavity of the chelating ligand helps in stabilising the terminal oxo complexes and this idea has been actively explored in the area of biomimetic chemistry.

In the literature, there are several experimental studies on the generation of Mn$^{III/IV}$–O(H) complexes using tripodal ligand. Shirin et al.[8] synthesised the Mn^{III}–O(H) complexes [Mn^{III}H$_3$buea(O)]$^{2-}$ and [Mn^{III}H$_3$buea(OH)]$^{-}$, (here buea = tris [(N′-tert-butylureayl)-N-ethyl]amine) using tripodal ligand and confirmed their formation by FTIR and X-ray diffraction measurements. They found the high spin state as the ground state configuration with effective magnetic moments of 4.92 and 4.90 μBM, respectively. Further, Gupta et al.[9] using water synthesised Mn$^{III/II}$–OH and Mn^{III}–O complexes to probe their reactivities and correlate the bond dissociation energies to the reactivity of Mn–Oxo species. MacBeth et al.[10] have synthesised a type of mononuclear Fe^{III} and Mn^{III} complexes with terminal oxo and hydroxo ligands directly from dioxygen and characterised them with IR, EPR, and X-ray studies to confirm the formation of M$^{III/IV}$–O(H) species. In this study, they have shown the formation of Mn^{IV}=O intermediates during the reaction, which is capable of abstracting hydrogen atoms from external sources, such as a solvent. Parsell et. al.[11] have shown the reactivity of monomeric Mn$^{III/IV}$–oxo complexes and role of the oxo ligand in either C–H bond cleavage or O-atom transfer reactions and they performed the kinetic analysis to determine the basicity of the Mn$^{III/IV}$–OH complex and they found the large value of the pK$_a$ for the [Mn^{III}H$_3$buea(OH)]$^{2-}$ ~28.3 than the [Mn^{IV}H$_3$buea(OH)]$^{2-}$. This result supports that the basicity has greater importance on the reactivity that involves the C–H bond activation.

A vast literature survey is accessible on the high valent-manganese oxo species,[2f,g,i,12] of particular interest is the ponderable efforts that have been devoted by Borovik and his coworkers, with tripodal ligand in the formation of Fe$^{II/III/IV}$/Mn$^{II/III/IV}$–O(H) because this specific choice of ligand exhibits characteristic of forming shielding hydrogen bond cavity around the metal–(OH) units to avoid the tendency to form μ-oxo bridged dimers.[3d,9–10,13] The main strategy of the experimental group is influenced by the hydrogen bonding phenomenon occurring in the native metalloproteins and the use of a chelating tetradentate tripodal tris[(N′-tert-butylureayl)-N-ethyl]amine (buea) ligand is supposed to provide a rigid hydrogen bonding framework involving metal–O(H) groups. The urea groups of the ligand create a cavity around the metal with three negatively charged and one neutral N donor sites protecting the metal from dimerisation resulting in the formation of terminal Mn–O species. Experimentally, the precursor [Mn^{II}H$_2$buea]$^{2-}$ is prepared from the reaction of the ligand with the acetate salt of the metal, Mn(OAc)$_2$, in the presence of solid KH (base) in dimethylacetamide (DMA) used as a solvent under Ar atmosphere. Dry molecular O$_2$ has been used for the source of the oxygen during the reaction. In one of the steps, H$_2$O has been added, and we supposed that it could help in the intermolecular transfer of hydrogen atom. Finally, Mn^{IV}=O is forming via one-electron oxidation of Mn^{III}=O, and experimentally Cp$_2$Fe$^+$ cation is used for this purpose.[10]

In recent years computational approaches to understand the electronic structure and mechanistic features are gaining attention in the area of high-valent heme and non-heme enzymes. In a very recent study,[14] carried out by our group, in which the hydrogen atom transfer (HAT) using [Mn^{III}H$_3$buea (O)]$^{2-}$ and [Mn^{IV}H$_3$buea(O)]$^{-}$ species have explored and suggested the possible mechanisms for HAT, to probe the role of basicity in deciding the course of C–H activation reaction.[14–15] In this direction, de Visser and his coworkers have made significant contributions to focus on the reactivity of high-valent manganese but with other ligand backbones, where they reported the oxidative abilities of the species involved in catalytic processes corresponds to cytochrome P450.[14–15] In another report by the same group, they elaborated hydrogen-bonding interactions to the metal oxo group and concluded that hydrogen bonding lowers the bond-dissociation energy BDE$_{OH}$ value and, consequently, the oxidative power of the oxidant. While most of the studies both on Fe–oxo and Mn–oxo focus on their electronic structure and reactivity, studies on the mechanism of formation of these species starting from simple Mn^{II}/Fe^{II} precursors are rare. In this work, we report the computational studies on the mechanism of the generation of the high-valent manganese species (Mn$^{III/IV}$=O) with tripodal ligand [H$_3$buea]$^{3-}$. In our mechanistic study, we have proposed a possible mechanistic pathway using O$_2$ as an oxidant and analysed the structure, bonding, and spin state energetic of all possible intermediates and transition states to offer insight, for the first time, on the formation of such species.

Full Paper

2. Computational Details

All calculations were carried out using the Gaussian 09[16] suite of program. All gas-phase geometry optimisations were performed without any restriction using the UB3LYP[17] level of theory. The 6-31G* basis set was used to describe the nonmetal atoms such as C, H, O, and N where the metal atom, i.e., Mn, is treated by LanL2DZ basis set with the treatment of electron core potential (ECP). Single point energy calculations were performed on the optimised geometries using a TZVP basis set for all atoms. Vibrational analysis at the same level of theory has been performed for all the optimised geometries and confirms the minima or saddle points (transition states) in the potential energy surface. All the transition states were characterised by only one imaginary frequency corresponding to the expected reaction coordinate and verified by animating the vibration mode using Chemcraft software. All the intermediate species on the potential energy surface possess only positive frequencies. The transition states were computed by a relax scan of a certain parameter such as bond length and angles along a potential energy surface or by computing molecular hessian corresponding to the geometry with maximum energy. All transition states and the intermediates were optimised without any restriction. Intrinsic reaction coordinate (IRC) calculation has been performed to evaluate the nature of the species connected by a given transition state (TS). The bulk solvent effect has been incorporated by the single point energy calculations using polarisation continuum solvent model (PCM)[28] with the same level of theory and TZVP basis set for all the atoms. Here we have used DMA (dimethylacetamide) as a solvent. We here included zero-point energy correction terms along with the free-energy corrections for the reaction energy calculations for all intermediates and the transition states on the potential energy surface for all the species unless otherwise menitioned. For ts2* (see below) however only electronic energy is considered as this is obtained from potential energy scan. To calculate energies of intermediate structures with degenerate spin states, fragment technique available in Gaussian 09 is used. All spectroscopic parameters (EPR parameters, absorption) were calculated using the ORCA Program Version 3.0.1.[29] We have incorporated relativistic effect via zeroth-order regular approximation method (ZORA) as implemented in ORCA suite.[18] The solvent effect has been incorporated using COSMO method.[19] DFT calculations have been performed for the estimation of the D-tensor with the B3LYP functional using quasi-degenerate theory with CP approach.[20] The TZVP basis set was used for all atoms. Increased integration grids (Grid 5 in ORCA convention) along with tight SCF convergence were used. Herein, we have used notations for all the species such as $^{2S+1}$[species name]$_{s(ij)}$, where, in the subscript, s is the spin state of the metal. In the parenthesis, i- denotes the spin of the deprotonated nitrogen $N_{\alpha'}$ of the ligand moiety next to the uryl methyl group (spin-up/spin-down) and j-denotes the spin for either O or in some cases C1 of DMA (H-donor) (spin-up/spin-down) while in the notation $^{2S+1}$[species name]$_{s(i)}$ i-

denotes the unpaired spin on the nitrogen $N_{\alpha'}$. For simplicity, we have denoted $N_{\alpha'}$ as N in all the figures. Also, spin-up and spin-down are denoted by "u" and "d" for simplicity throughout the manuscript.

3. Results and Discussion

The synthesis and reactivity of the various intermediate involved in the generation of the Mn$^{III/IV}$–oxo species were reported by Borovik and coworkers.[10] Based on the above experimental evidence, we have proposed the mechanism for the formation of monomeric Mn$^{III/IV}$–oxo complexes with the tripodal ligand [tris[(N′-tertbutylureaylato)-N-ethyl]aminato, (H$_3$buea^{3-}) using density functional theory calculations (Scheme 1). The proposed mechanism, which involves the various intermediates and transitions states, has been depicted in Scheme 1.

According to Scheme 1, The reaction initiates by the formation of a Mn^{III}–superoxo species, which is formed by the reaction of the catalyst species [Mn^{II}H$_2$buea]$^{2-}$ (*R*) and molecular oxygen. Here we expected that the negatively charged nitrogen atom (N$_{\alpha'}$, denoted by N in all the figures, see Figure S1) of one of the urea ligand would donate one of the radical to the Mn^{III} centre making it Mn^{II} and the resulting complex will be [Mn^{II}H$_2$buea(OO)]$^{2-}$(*int1*). This superoxo species expected to abstract hydrogen from DMA (solvent) to form the [Mn^{II}H$_2$buea(OOH)]$^{2-}$ (*int2*) complex. This complex again abstracts a proton from either DMA solvent or H$_3$O$^+$ ion present which simultaneously leads to the elimination of water molecule from [Mn^{II}H$_2$buea(OOH$_2$)]$^-$. After elimination of water molecule, [Mn^{III}H$_2$buea(O)]$^{2-}$(*int4*) complex is formed. The Mn^{III}=O species will again abstract hydrogen from the solvent, which leads to the formation of [Mn^{II}H$_2$buea(OH)]$^{2-}$ (*int5*) complex. The Mn(II)–hydroxo species has been accomplished by the intramolecular hydrogen atom transfer towards the endogenous basic nitrogen N site (N$_{\alpha'}$) in the cavity, which is in close proximity to the hydroxide moiety resulting in the formation of [Mn^{III}H$_3$buea(O)]$^{2-}$(*int6*). Finally, the Mn^{IV}–oxo species (*P*) could be formed from the precursor Mn^{III}–oxo species using oxidants, which is a one-electron redox process. The stepwise formation of different species, along with their transition states, will be discussed in the following section of the manuscript.

Formation of superoxide species, [Mn^{II}H$_2$buea(OO)]$^{2-}$ (int1) from free reactant [Mn^{II}H$_2$buea]$^{2-}$ (R): As depicted in Scheme 1, the calculations have been initiated with the approach of the catalyst, [Mn^{II}H$_2$buea]$^{2-}$ towards molecular oxygen and the developed potential energy surface is given in Figure 1. We have optimized the geometries of [Mn^{II}H$_2$buea]$^{2-}$ in all the three possible spin states (S = 5/2, S = 3/2, and S = 1/2). From the DFT calculations, it is predicted that the catalyst possesses a high spin, S = 5/2, $^6R_{hs}$ state as the ground state while the other intermediate energy states, i.e., S = 3/2 ($^4R_{is}$) and S = 1/2 ($^2R_{ls}$) are lying 115.1 kJ/mol and 176.1 kJ/mol higher in energy than the ground state respectively (see
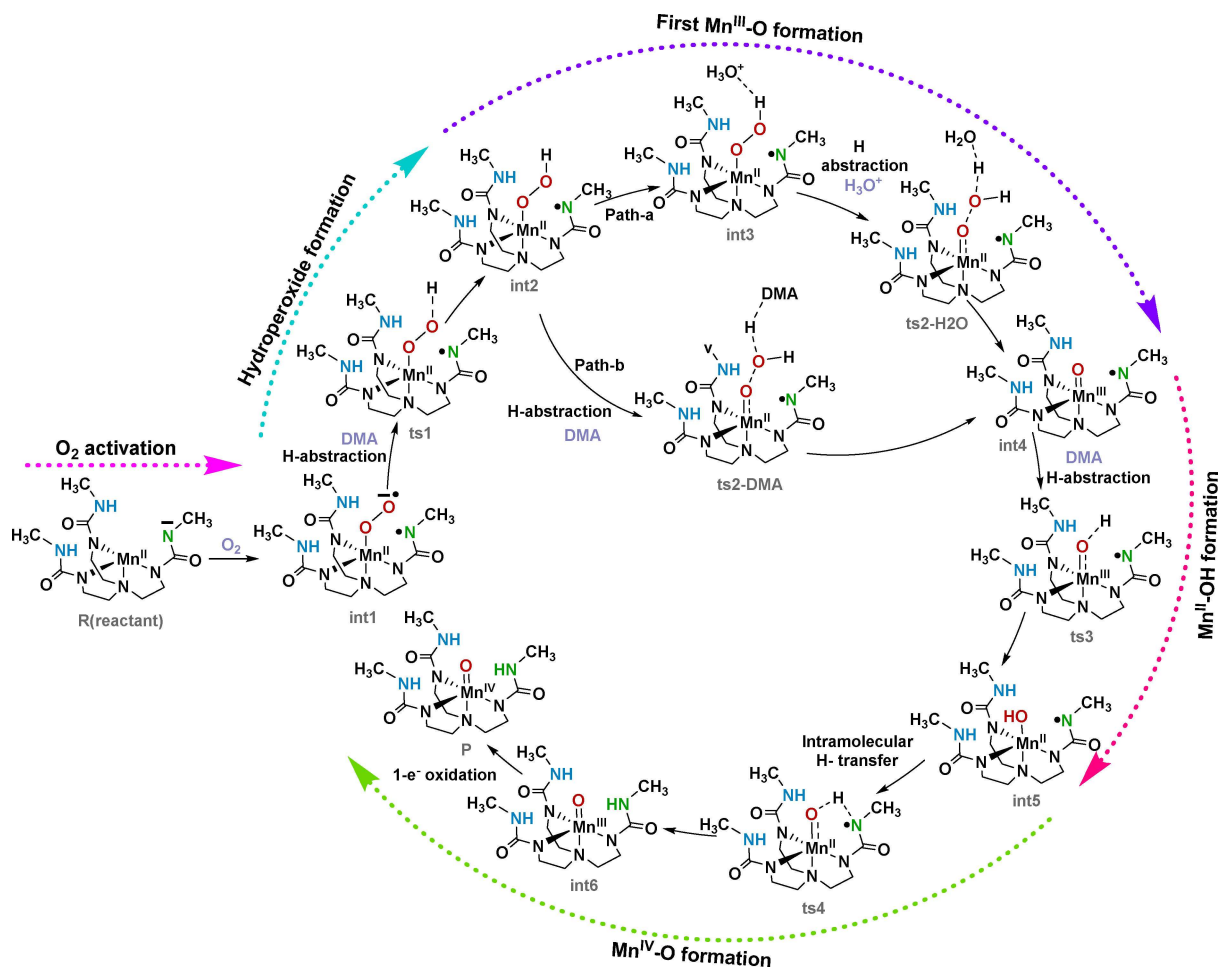
Scheme 1. Schematic diagram for the formation of Mn$^{III/IV}$—oxo species from [Mn^{II}H$_2$buea]$^{2-}$. Here, DMA stands for dimethylacetamide which is used as solvent here.

Figure 1). The spin density values on the Mn^{II} centre are 4.809, 3.013, 1.011 in the $^6R_{hs}$, $^4R_{is}$, $^2R_{ls}$ spin states respectively, which is indicative of the 5, 3, and 1 number of unpaired electrons, respectively (see Figure 2). These high lying S = 3/2 and S = 1/2 states are therefore excluded for our further calculations. The average distance between the metal centre and the equatorial deprotonated nitrogen atoms, (Mn–N$_{equi}$) in the ground state is found to be in between 2.08 Å to 2.19 Å which is much lower than that of the distance of the metal centre and the axially ligated N atom (2.52 Å) (see Figure 2). This is indicative of a distorted structure due to the presence of different types of donors in the molecule. The support for the S = 5/2 ground state of the catalyst species comes from X-band EPR measurement, although this was done with [Mn^{II}H$_2$bupa]$^-$ complex. It reveals that the complex as a nearly axial S = 5/2 spin has a zero-field splitting constant of D∼ 0.3 cm^{-1} with the E/D∼0.002062 cm^{-1},[21] and our computed D values are noted to be ∼0.45 cm^{-1}. Also, the large value of the rhombic parameter indicates lower symmetry around the metal center or this ligand providing a more unsymmetrical

environment than [H$_3$bupa]$^{3-}$ ligand. While accurate estimation of zero-field splitting parameters require ab initio CASSCF approach, the high-spin S = 5/2 do not have any d-electronic excited states and therefore contribution coming from the higher excited states and spin-orbit coupling is expected to be small and negligible with the main input to D expected to arise from spin-spin contribution which is well captured within DFT formalism as stated earlier.[22]

The tetra-anionic ligand complexed with Mn^{II} centre in the first step simultaneously reacts with molecular oxygen in DMA solvent under an argon atmosphere in the presence of a solid KH base resulting in the formation of a superoxo species (*int1*). However, the spin density values confirm that the metal atom is not oxidised during the superoxide formation, and it is due to the single-electron transfer from the anionic end of the nitrogen (denoted by N, see supporting information, Figure S1) to the Mn centre during the course of the reaction, keeping intact the oxidation state of the metal. This also results in a simultaneous reduction of spin density on the nitrogen centre (N), generating a radical. A radical centre at the
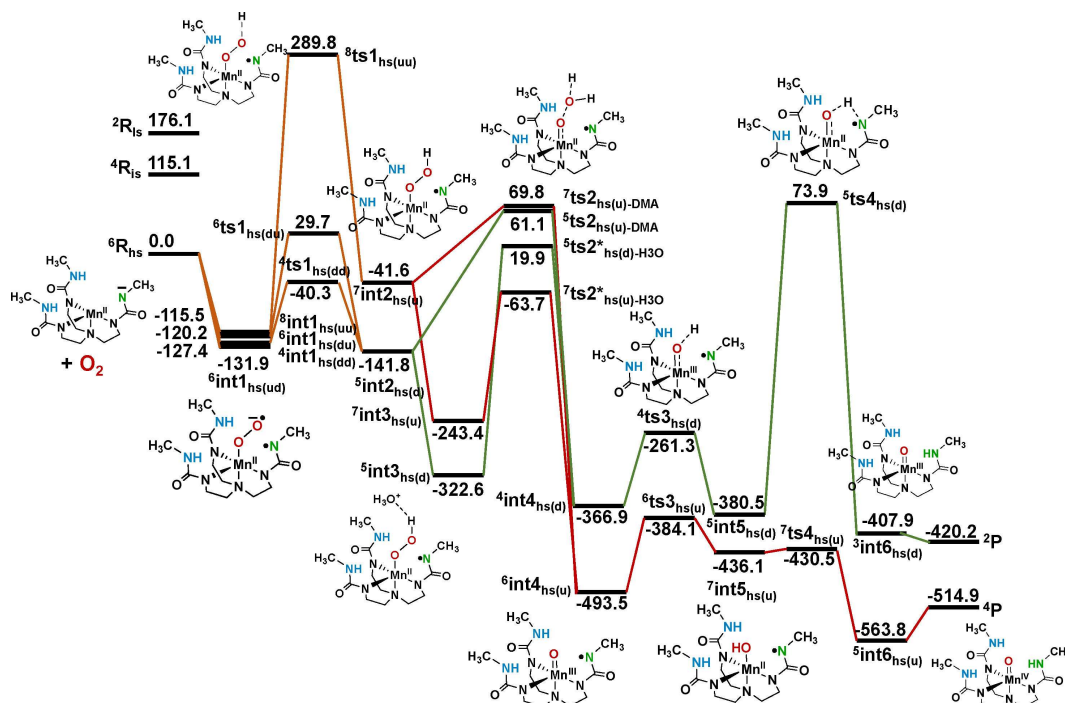
These are not the final page numbers! ↗↗

Figure 1. Potential energy surface for the reactions as depicted in Scheme 1. All the energies are in kJ/mol. Red lines corresponds to radical spin-up on $N_{\alpha'}$ and green corresponds to radical spin-down on $N_{\alpha'}$. Note in this figure different spins are related for the sake of simplicity only considering the spin of the metal centre and the ligands in the primary coordination sphere. Herein, ts2* indicates that it is not the actual saddle point in the potential energy surface, see computational detail for more discussion.
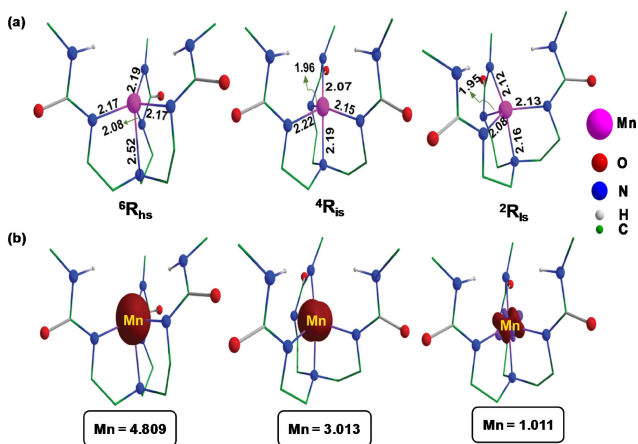
Figure 2. (a) DFT optimized geometry of the free catalyst [MnH₂buea]²⁻ in the S=5/2 ($^6R_{hs}$), S=3/2 ($^4R_{is}$), S=1/2 ($^2R_{ls}$) states respectively showing important bonding parameters and (b) spin density plots of the respective spin states.

nitrogen atom is justified as the protonation of all the nitrogen present in the ligand found to not to generate the desired Mn^{IV}=O species in the experiments[10] suggesting the importance of the one of the nitrogen to be deprotonated which as per our calculations (see below) develops significant radical character upon oxygen activation. To ascertain whether this radical formation at the ligand is due to issue of the functional used,

we have carried out geometry optimisation for this intermediate (*int1*) in different level of theory such as TPSSH and PBE0 and these calculations also offer results which are similar to B3LYP functional. The spin density values of *int1* in the PBE0 and TPSSH level is tabulated in Table S2 and Table S3 (see supporting information). Considering a high-spin Mn^{II} with a radical on the superoxide moiety as well as on the newly oxidised nitrogen atom (denoted by *N)* in *int1*, DFT calculations reveal that $^6int1_{hs(ud)}$ state, where the radical on the nitrogen N is spin-up, and that of superoxo species is spin-down is found to be the most stable by 131.9 kJ/mol lower energy than the reactant species. Other spin states, i.e., $^8int1_{hs(uu)}$ (both the radicals on oxygen and the nitrogen N are spin-up), $^6int1_{hs(du)}$ (the radical on nitrogen is spin-down, and that of oxygen is spin-up), $^4int1_{hs(dd)}$ (both the radicals on oxygen and the nitrogen are spin-down) are lying 16.4, 11.7, 4.5 kJ/mol higher from the ground state $^6int1_{hs(ud)}$ (see Figure 1). All four states computed are close lying in energy and could contribute further to the reactivity. In low lying $^6int1_{hs(ud)}$ state, a spin density of 4.687 on the Mn centre, −0.337 and −0.464 on the proximal (O1) and distal oxygen (O2) atoms of superoxide moiety respectively and a significant positive spin density of 0.915 on the N atom have been observed (see Figure 6). The spin densities on the respective atoms of the other high-lying states are given in Figure S2(b). The Mn–O bond distance of 2.06 Å and O–O distance of 1.34 Å in the ground state is indicative of the Mn^{II}–O single bond character, and slight

elongation in the O–O distance is due to a radical, anionic character on the distal O atom. The average O–O distance in all four spin states is between 1.34 Å to 1.35 Å. In all the four possible spin states of *int1*, the average equatorial Mn–N$_{equi}$ (N$_{equi}$ = N1, N3, and N4) bond distances are between 2.17 Å to 2.22 Å, whereas the Mn–N$_{axial}$ bond distances vary from 2.42–2.57 Å (see supporting information, Figure S2(a)). The occupation of five electrons in $^6int1_{hs(ud)}$ state is found to be in $\pi^*_{yz}{}^1$ $\pi^*_{xz}{}^1$ $P_{(N)}{}^1$ $\pi^*_{(O-O)}{}^{-1}$ $\delta_{x2-y2}{}^1$ $\delta_{xy}{}^1$ $\sigma^*_{z\,2}{}^1$ (see supporting information, Figure S14). The π^*_{yz} and π^*_{xz} orbitals are non-degenerate by 0.06 eV while the degeneracy of the δ orbitals is lifted by ~0.2 eV and lies 2.47 eV higher than that of lowest π^*_{yz} orbital. The $\sigma^*_{z\,2}$ orbital is the most destabilised among all and lies at 2.89 eV compared to π^*_{yz} orbital.

Formation of hydroperoxide species, [Mn^{II}H$_2$buea (OOH)]$^{2-}$(int2): The formation of superoxide intermediate, [Mn^{II}H$_2$buea(OO)]$^{2-}$ (*int1*) is then followed by the abstraction of hydrogen from DMA, which is present in the reaction medium as a solvent, which results in the formation of a Mn^{II}–hydroperoxo species, [Mn^{II}H$_2$buea(OOH)]$^{2-}$ (*int2*) through a hydrogen transfer transition state *ts1 (int1→int2)*. The lowest energy barrier for the hydrogen atom abstraction step is found to be 87.1 kJ/mol in the quartet energy surface, $^4ts1_{hs(dd)}$ with the spin-down on radical both on the superoxide and on the nitrogen N atom in S = 5/2 surface of Mn^{II} ion. This hydrogen abstraction step is highly energy demanding in other spin surfaces. The transition energies associated with the states, $^8ts1_{hs(uu)}$, $^6ts1_{hs(du)}$ are very high, and lying uphill by an amount of 330.1, 70.0 kJ/mol than $^4ts1_{hs(dd)}$ in the potential energy surface. From these energy values, we can conclude that although $^6int1_{hs(ud)}$ is the lowest energy point in the potential energy surface for *int1*, the reaction will proceed via $^4int1_{hs(dd)}$

state, which is associated with the lowest barrier of 87.1 kJ/mol. From the energetics, it is seen that the transition state, $^4ts1_{hs(dd)}$ is exergonic by 40.3 kJ/mol than that of the ground state S = 5/2 of the catalyst, [Mn^{II}H$_2$buea]$^{2-}$, which is indicative of a barrierless process from the free reactant. From the values, it is obvious that the reaction will not be feasible through the potential energy surface corresponding to $^8ts1_{hs(uu)}$ state due to prohibitively high energy barrier. The spin density of −0.706 on the C1 atom of the DMA molecule in the transition state, $^4ts1_{hs(dd)}$ indicative of the transfer of α-electron from DMA to the N atom reducing its spin density to nearly zero and at the same time spin density on the metal is reduced by 0.48 units (see Figure 3). Schematic MO diagrams of $^4int1_{hs(dd)}$ and $^4ts1_{hs(dd)}$ are shown in Figure 4 in the manuscript, and from the diagram, it is seen that $^4int1_{hs(dd)}$ has the following electronic configuration $\pi^*_{(O-O)}{}^{-1}$ $\pi^*_{xz}{}^1$ $\pi^*_{yz}{}^1$ $P_{(N)}{}^1$ $\delta_{xy}{}^1\delta_{x2-y2}{}^1$ $\sigma^*_{z\,2}{}^1$ while after transferring a α-spin from the σ_{C-H} bond to the $P_{(N)}$ orbital (the pure P orbital on the nitrogen N atom which is indicative from the reduction of spin density on the nitrogen N during the transition) during the transition state, the electronic configuration at the transition state becomes $P_{(N)}{}^1$ $\delta_{xy}{}^1\pi^*_{yz}{}^1\delta_{x2-y2}{}^1$ $P_{(N)}{}^{-1}$ $\pi^*_{(O-O)}{}^{-1}$ $\pi^*_{xz}{}^1$ $\sigma^*_{z\,2}{}^1$. The hydroperoxo–Mn^{II} species (*int2*) possesses two possible spin states with the Mn^{II} centre in the high-spin (S = 5/2) state, the lowest energy $^5int2_{hs(d)}$ state which is slightly exergonic by 14.4 kJ/mol than that of $^4int1_{hs(dd)}$ while the high lying septet energy state ($^7int2_{hs(u)}$) is highly endergonic by 85.8 kJ/mol. From the energetics, we can conclude that the reaction will proceed through the quintet energy surface. In *int2*, the O–O bond is elongated by 0.14 Å in the septet state, where the elongation is much less in the quintet state by an amount of 0.02 Å compared to the *int1* (see supporting information, Figure S4 and Figure 5).
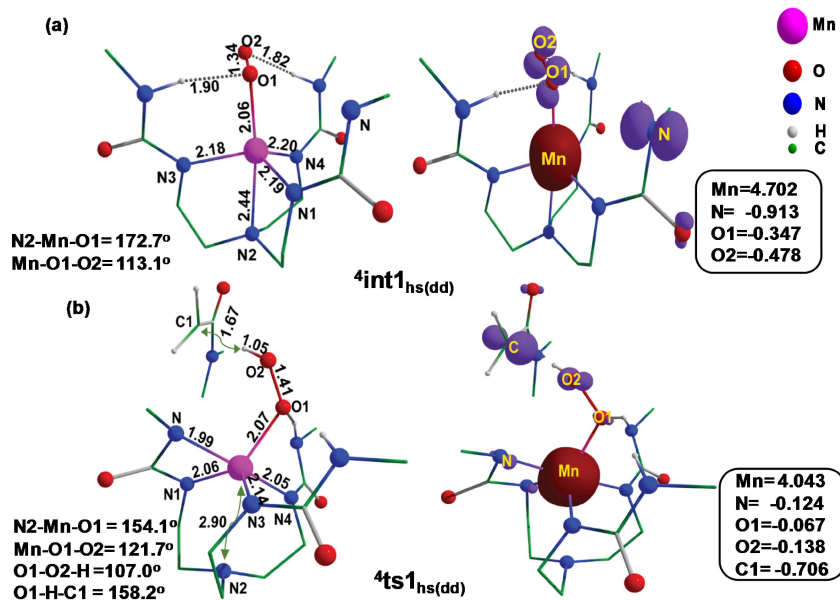

Figure 3. DFT optimized structure of (a) $^4int1_{hs(dd)}$ with important bonding parameters and its respective spin density plot and (b) $^4ts1_{hs(dd)}$ with important bonding parameters and its respective spin density plot.
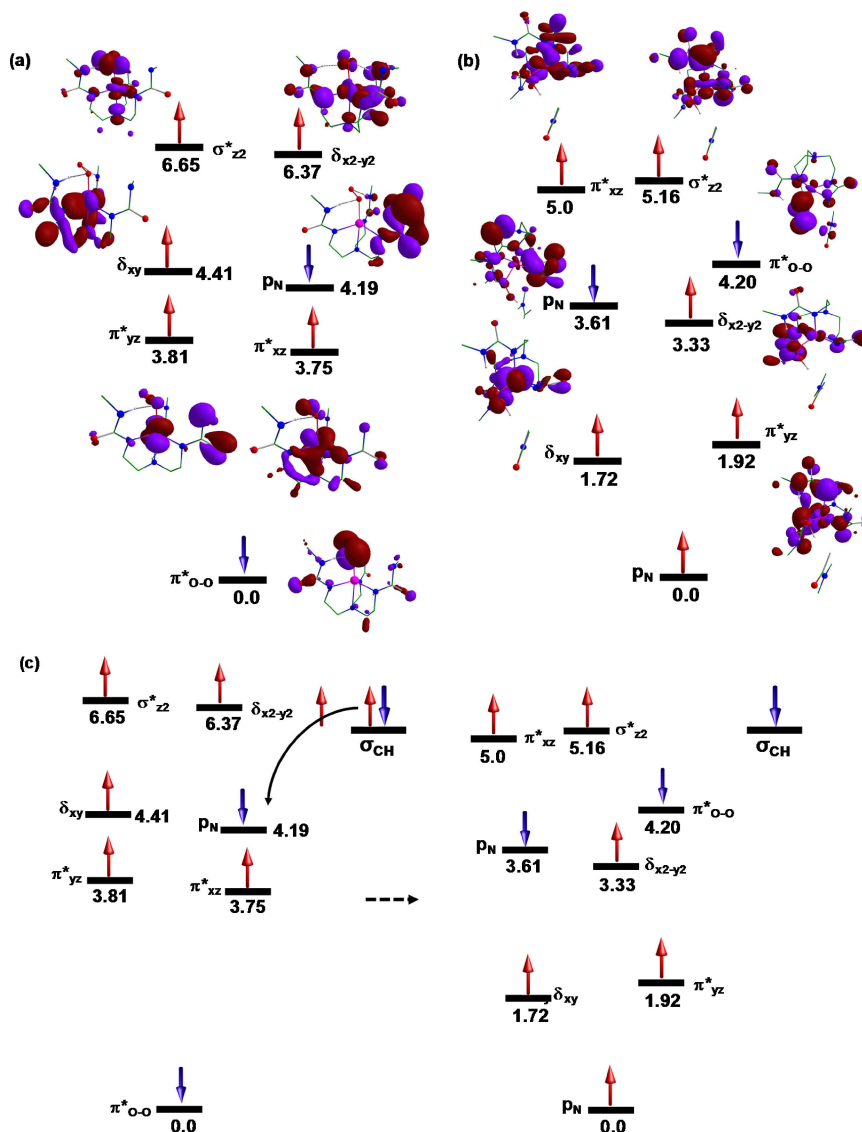
Figure 4. (a) Schematic MO diagrams of species $^4int1_{hs(dd)}$ and (b) Schematic MO diagrams of species $^4ts1_{hs(dd)}$ (c) The feasible electron shifts between the σ_{C-H} bond and the Mn–O d-based orbitals during the corresponding transition.

The average $Mn^{II}–N_{equi}$ (N_{equi} = N1, N3, N4) distance is found to be in between 2.16 Å to 2.23 Å while the axial $Mn^{II}–N2$ bond length is decreases comparatively than the previous states (*int1*) to 2.39 Å in S = 2 spin states, respectively. The spin density values reveal a significant amount of α- spin of 0.733 on the N atom in the septet state while in the quintet state there is no β- spin on the N nitrogen but a small amount of negative spin is observed on the O1 (−0.289) and O2 (−0.333) atoms. Also, the spin density is slightly reduced to 4.520 on the Mn centre $^5int2_{hs(d)}$, and all these facts are indicative towards the transfer of β- spin from the N nitrogen centre to the metal as well as to the oxygen atoms (see Figure 6). In *int2*, the lower Mn–O bond length of 1.97 Å (see Figure 5)in the lowest energy quintet state than that of Fe–O

distance of 2.014 Å[23] in the previously reported complexes implies towards comparatively stronger Mn–O interactions.

Formation of [$Mn^{III}H_2buea(O)$]$^{2-}$ (int4) species: Now from *int2*, there are two possible pathways that lead to the formation of *int4*, [$Mn^{III}H_2buea(O)$]$^{2-}$. Firstly, the *int2* can abstract another hydrogen as H^+ from the water molecule that is available in the precursor metal salts used, or it can abstract H^+ from the solvent molecule, DMA. In the first pathway, a large energy gain has ensued when the *int2* forms hydrogen-bonding interaction with the cage leading to the formation of *int3* (243.4 kJ/mol and 322.6 kJ/mol in the septet ($^7int3_{hs(u)}$) and quintet ($^5int3_{hs(d)}$) energy surface, respectively). The reduced spin density of 3.962 on the Mn^{II} centre and also no β- spin on the N atom in $^5int3_{hs(d)}$ indicative of the transfer of the β-electron to the metal lowering significantly the spin density
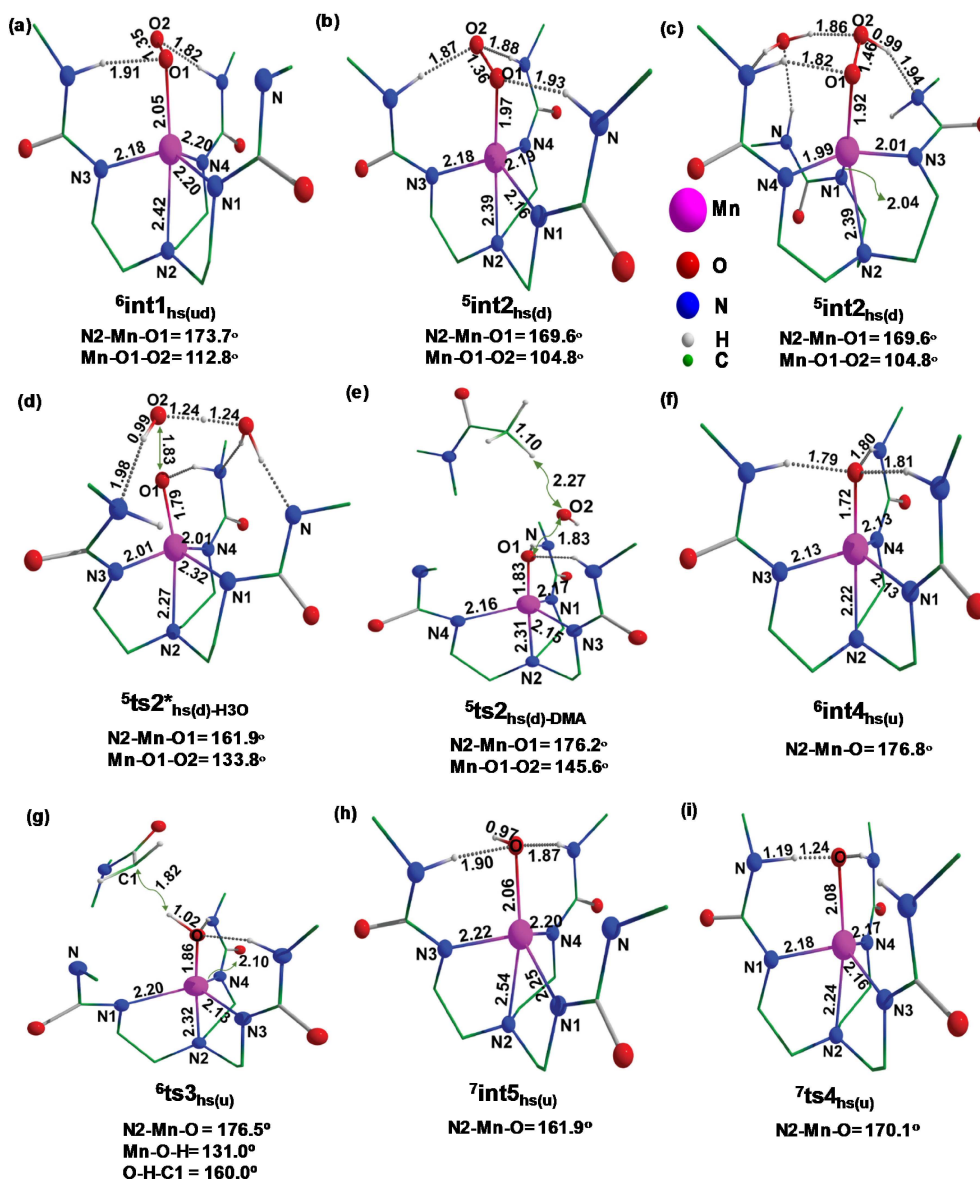
Figure 5. DFT optimized structure showing important bond parameters of (a) $^6int1_{hs(ud)}$, (b) $^5int2_{hs(d)}$, (c) $^5int3_{hs(d)}$, (d) $^5ts2*_{hs(d)-H3O}$, (e) $^5ts2_{hs(d)-DMA}$, (f) $^6int4_{hs(u)}$, (g) $^6ts3_{hs(u)}$, (h) $^7int5_{hs(u)}$, (i) $^7ts4_{hs(u)}$.

on Mn atom (see Figure 6) while in the S = 3 state the β-spin on the N has not transferred to the Mn but to the other N groups of the buea ligand (see supporting information, Figure S5). In the preceding step, *int3* is involved in a simultaneous bond-breaking and making process, which is associated with *ts2*. In *ts2*, the O2 atom of the hydroperoxo unit attacks a hydrogen ion from the donor species and at the same time, simultaneously involved in the O1–O2 bond-breaking process leading to the formation of *int4*. Now the second proton transfer from the H_3O^+ ion present in the system is associated with the intrinsic barrier of 179.7 kJ/mol in the septet energy surface while that the quintet state is associated with a 342.5 kJ/mol higher barrier than that of the septet (see Figure 1). This is because hydrogen bonding lowers

the energy of the quintet state, $^5int3_{hs(d)}$ by 79.2 kJ/mol more than that of the septet, and this reveals that the H-bonding interactions and the associated stabilisation are strongly correlated to the spin-states. Our attempts to optimise *ts2* in septet and quintet energy surface were not successful. To obtain a realistic estimate of barrier heights on these surfaces, we have performed a relaxed potential energy scan along the O1–O2 bond ranging from 1.16 Å to 1.25 Å, and the highest energy point on the potential energy scan graph has been taken for the single point energy calculations to estimate the maximum energy barrier at this potential energy surface (see supporting information, Figure S15). For both the $^7ts2*_{hs(u)-H3O}$ and $^5ts2*_{hs(d)-H3O}$ states, the critical O1–O2 bond length is found to be 1.83 Å, and the newly forming O–H bond

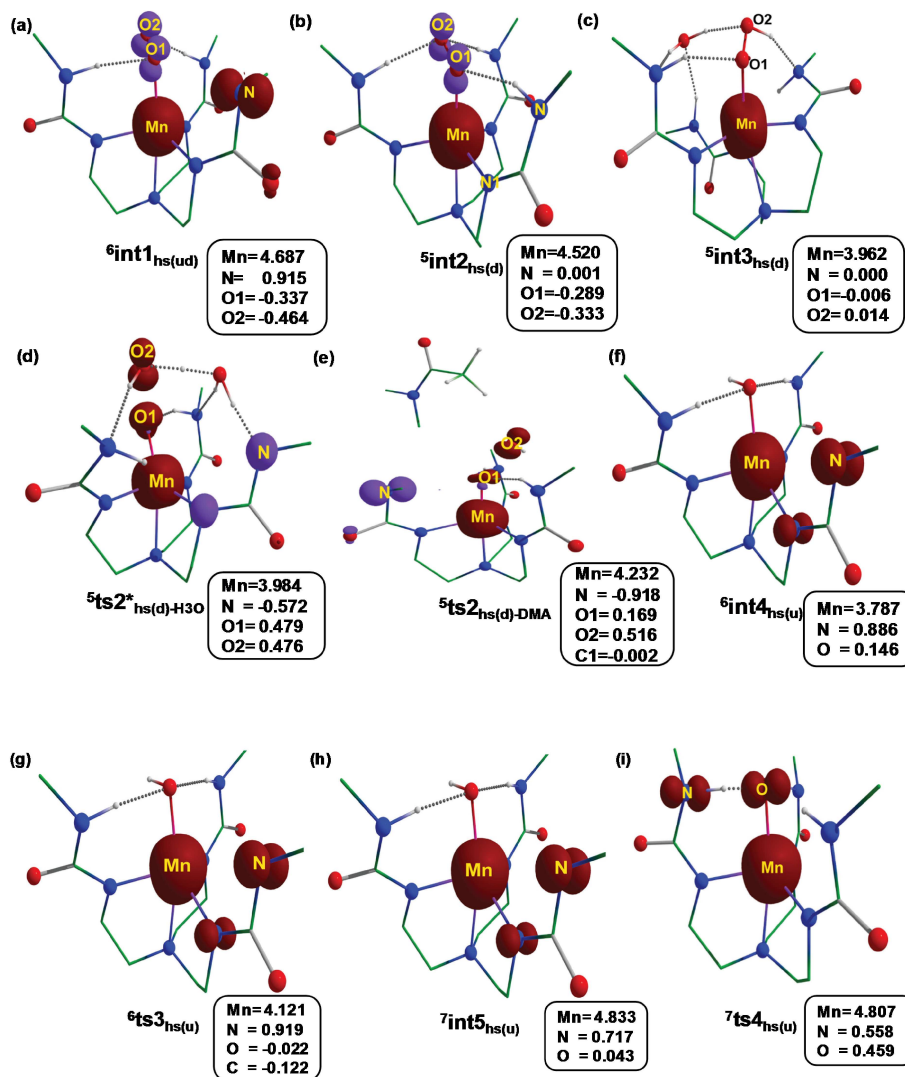**Figure 6.** DFT computed spin densities of (a) $^6int1_{hs(ud)}$, (b) $^5int2_{hs(d)}$, (c) $^5int3_{hs(d)}$, (d) $^5ts2*_{hs(d)-H3O}$, (e) $^5ts2_{hs(d)-DMA}$, (f) $^6int4_{hs(u)}$, (g) $^6ts3_{hs(u)}$, (h) $^7int5_{hs(u)}$, (i) $^7ts4_{hs(u)}$.

distances are 1.25 Å and 1.24 Å, respectively in the limiting state. In the transition state *ts2*, Mn–O1 bond length is found to be decreased to 1.83 Å and 1.79 Å in the $^7ts2*_{hs(u)-H3O}$ and $^5ts2*_{hs(d)-H3O}$ states from 2.03 Å and 1.92 Å in the $^7int3_{hs(u)}$ and $^5int3_{hs(d)}$ states respectively, and the transition O–O bond length of 1.83 Å is indicative of the fact that Mn–O bond is getting shorter than a single bond but longer than a double bond (see Figure 5 and supporting information, Figure S6(a)). The $^7ts2*_{hs(u)-H3O}$ and $^5ts2*_{hs(d)-H3O}$ states possess an α-spin of 3.991 and 3.984 on the Mn-center along with the 0.601 and −0.574 spin densities on the N atom respectively. A significant amount of spin densities of 0.693/0.574 and 0.479/0.476 are found on the O1/O2 atoms in the respective $^7ts2*_{hs(u)-H3O}$ and $^5ts2*_{hs(d)-H3O}$ states, which conclude the process of α-spin transfer to these oxygen atoms from the metal centre as a result of lowering the α-spin density on the metal (see Figure 6 and supporting information, Figure S6(b)). Another important

aspect in *ts2* is the decrease in the Mn–N$_{axial}$ bond lengths to a much shorter range of 2.19 Å and 2.27 Å in $^7ts2*_{hs(u)-H3O}$ and $^5ts2*_{hs(d)-H3O}$ respectively (see Figure 5 and supporting information, Figure S6(a)).

The second possibility for the same is a direct hydrogen transfer from the DMA (present in the reaction mixture) to *int2* without any involvement of the crystallographic waters (avoiding the formation of *int3*, path-b in the Scheme 1). In this case, the activation barrier for the hydrogen transfer is found to be 111.4 kJ/mol and 202.9 kJ/mol from the *int2* in the septet and quintet energy surface, respectively. In the *ts2*, the concern O1–O2 bond length is 1.82 Å and 1.83 Å respectively in the septet and quintet energy surface while that between H and O2 are 2.29 Å and 2.27 Å respectively. In the transition state, the C–H bond is slightly elongated to 1.10 Å in both cases (see Figure 5 and supporting information, Figure S7(a)). Also, the negative frequency of 600 cm^{-1} is mainly associated

These are not the final page numbers! ↗↗

with the O1–O2 bond cleavage, and these bond length parameters and frequencies are indicating a long-range hydrogen transfer from the DMA to O2; firstly, the O1–O2 bond will cleave and newly formed OH$^-$ will simultaneously accept hydrogen from DMA resulting in the formation of *int4*. The spin densities on the Mn centre/N radical are 4.248/0.910 and 4.232/−0.918 in the $^7ts2_{hs(u)-DMA}$/$^5ts2_{hs(d)-DMA}$ respectively (see Figure 6 and supporting information, Figure S7(b)). We have also calculated the deformation energies of the two transition states corresponding to two different pathways. However, the barrier of $^7ts2^*_{hs(u)-H3O}$ and $^5ts2^*_{hs(d)-H3O}$ is lower than that of the DMA. Similarly, deformation energies are also similar for $^7ts2^*_{hs(u)-H3O}$/$^7ts2_{hs(u)-DMA}$ (48.8/46.7 kJ/mol) while that of in the quintet energy surface are 63.7 kJ/mol and 68.9 kJ/mol respectively. From these values, we can conclude that it is the hydrogen-bonding network present in *int3* as well as *ts2*-H2O*, which controls the rate of the hydrogen transfer. Both possible mechanisms collapse in the next step to *int4*, i.e. the first Mn^{III}–O species in the reaction pathway. Formation of *int4* is highly exergonic by −493.5 kJ/mol and −366.9 kJ/mol than that of the reactant in the septet and quintet potential energy surface, respectively. In $^6int4_{hs(u)}$ and $^4int4_{hs(d)}$, a significant amount of spin density is observed having values 3.787 and 3.784 respectively on the Mn^{III} indicating the presence of four unpaired α-spins on the centre. These two spin density values, along with the 0.886 and −0.821 spin on the respective N atoms indicate a very less delocalisation of the spins in *int4* (see Figure 6 and supporting information, Figure S8(b)). The Mn^{III}=O distance is found to be 1.71 Å in both the spin states, which is lower compared to the normal Fe^{III}=O bond length.[23b] The decrease of the Mn–O bond length to 1.72 Å from 1.83 Å in *ts2* points toward the formation of a strong Mn–O double bond (see Figure 5). In the preceding step, the oxo-group in *int4* will abstract a hydrogen atom again from the DMA molecule, eventually forming int5, [M^{II}H2buea (OH)]$^{2-}$.

Formation of [Mn^{II}H$_2$buea(OH)]$^{2-}$(int5) species: The formation of *int4→int5* is associated with the transition state *ts3*, which has a barrier of 105.6 kJ/mol in the quartet surface. The barrier associated with the quintet surface is 109.4 kJ/mol from *int4* (see Figure 1). Here also we have found a similar value of deformation energies of 56.8 and 59.5 kJ/mol for septet and quintet species respectively. From the spin density plot of $^4ts3_{hs(d)}$, we can observe a slight increase of spin density on the metal (4.118, implies to ~five α-spins) while a significantly low negative spin (−0.124) on the C1 carbon of DMA from where the hydrogen is supposed to transfer (see supporting information, Figure S9(b)). The Mn–O bond length of 1.86 Å in both the spin states along with a 1.02 Å length of O–H bond and the 1.82 Å/1.83 Å ($^6ts3_{hs(u)}$/$^4ts3_{hs(d)}$) separation between the C1 carbon and O unit directs to a late transition state where already the C1–H bond is broken completely, and O–H bond is started to form (see Figure 5 and supporting information, Figure S9(a)). In *int5*, Mn–O(H) bond length is found to be 2.06 Å, which is due to the newly forming Mn–O single bond (see Figure 5). A significant amount of Mn/N spin

density of 4.833/0.717 and 4.793/−0.601 in found in $^6int5_{hs(u)}$ and $^4int5_{hs(d)}$, respectively (see supporting information, Figure S10).

Formation of [Mn^{IV}H$_3$buea(O)]$^{1-}$ (P) species: The formation of the [Mn^{IV}H$_3$buea(O)]$^{1-}$ complex is accomplished by first the intramolecular hydrogen atom transfer between the −OH group and the anionic nitrogen end (N) and further the *int6*, [Mn^{III}H$_3$buea(O)]$^{2-}$ complex forms the [Mn^{IV}H$_3$buea (O)]$^{2-}$ after reduction using the highly oxidising reagent Cp$_2$Fe$^+$. To calculate the oxidized product energy, we have computed the energy of the corresponding Cp$_2$Fe$^+$/Cp$_2$Fe redox couple and calculated the thermodynamic energy penalty due to the oxidation without computing any barrier heights associated with this process. Here, in the *int5*, Mn atom is in +2 oxidation with its −OH group from which the hydrogen is being transferred to the mono-radical nitrogen atom (N) in a homolytic cleavage mechanism via *ts4* (*int5→int6*) resulting in the formation of *int6*. Again in *ts4*, Mn is in the +2 oxidation state, and it can couple with the mono-radical N centre ferromagnetically as well as antiferromagnetically generating two spin-states, $^7ts4_{hs(u)}$ and $^5ts4_{hs(d)}$ respectively. The intrinsic barrier for this intramolecular hydrogen transfer is lowest in the septet energy surface with an energy of 5.6 kJ/mol while the barrier is significantly high in case of $^5ts4_{hs(d)}$ and it is lying 454.4 kJ/mol higher than the corresponding $^5int5_{hs(d)}$ state. This barrier is prohibitively high for the reaction to proceed, and hence one can safely ignore this transition state. The −O–H bond distance of 0.97 Å in *int5* is elongated to 1.24 Å in $^7ts4_{hs(u)}$ (see Figure 5)and 1.39 Å in $^5ts4_{hs(d)}$ towards the radical nitrogen end and forms a weak bond of distance 1.19 Å and 1.24 Å respectively (see supporting information, Figure S11(a)). The above bonding parameters confirm that $^7ts4_{hs(u)}$ is early and that of $^5ts4_{hs(d)}$ is late transition state where in $^5ts4_{hs(d)}$ the proton is already transferred to the N end but not in $^7ts4_{hs(u)}$. Spin density values have shown a value of 4.807 and 3.820 on Mn in $^7ts4_{hs(u)}$ and $^5ts4_{hs(d)}$, respectively, while a value of 0.558 and 0.010 spin on the respective Ns (see Figure 6 and supporting information, Figure S11(b)) . A reduction in spin density in the quintet surface is due to the transfer of negative β-spin from the N end to the metal centre. Moreover, the manganese oxygen distance is shortened to 1.75 Å in the quintet surface, indicating the formation of the weak double bond. Now the transfer of hydrogen atom leads the formation of the complex [Mn^{III}H$_3$buea(O)]$^{2-}$. In the *int6*, Mn ion is in the +3 oxidation state with no significant radical character on the N atom. However, the formation of *int6* is exothermic by 127.7 kJ/mol for the quintet surface and slightly exothermic 27.4 kJ/mol in triplet surface from their corresponding *int5* species, respectively. These energetics are in broad agreement with the earlier preliminary study on the intramolecular hydrogen transfer by MacBeth et al..[10] In the last step of the mechanism, the formation of the [Mn^{IV}H$_3$buea(O)]$^{1-}$ (product) has been explained, which is the one-electron redox process at −0.076 mV versus Cp$_2$Fe$^+$/Cp$_2$Fe, which consequently forms the product P, [Mn^{IV}H$_3$buea(O)]$^{1-}$ complex by using the

internal oxidant.[10,26] The formation of P is slightly exothermic by 12.3 kJ/mol in doublet energy surface while in quartet surface it is endothermic by 48.9 kJ/mol (see Figure 1). The computed value of spin on the Mn is found to be 2.796, and on the oxygen atom, it is 0.231 in the high spin state while on the low spin state it is 0.909 on Mn and 0.103 on the oxygen atom (see Figure 7 and supporting information, Figure S13).

Spectral Characteristics of [Mn$^{III/IV}$H$_3$buea(O)]$^{2-/-}$: From the spin density plots, it is clear that the Mn contains four unpaired electrons in ^{5}*int6* with an α-spin value of 3.785, and in ^{3}*int6* the value is 1.977, indicating two unpaired electrons. The remaining spin delocalised to the ligand, although no significant spin on O atom is observed. From the DFT study of vibrational analysis, a strong vibration is assigned to ν(Mn−O) bond at 781.3 cm^{-1}, which is in agreement with the experimental value, i.e., ν(Mn−O) of 700 cm^{-1}.[10] Moreover, a strong vibrational feature was observed for Mn^{IV} in Mn^{IV}=O porphyrins at 754 cm^{-1}[24] and for Mn^{V} complex at 979 cm^{-1},[25] which is characteristic of multiple bonds between manganese and oxo ions. For the [Mn^{III}H$_3$buea(O)]$^{2-}$ complex, the Mn−O bond length is computed to be 1.72 Å, and this is consistent with experimental data reported from XRD (1.771 Å) and from earlier DFT (1.746 Å) study,[10] this distance span within the range seen for the complex Mn^{III}−O−M^{III}.[10,30] In ^{5}*int6* species, the three deprotonated urea nitrogen defines the trigonal planes with an average Mn−N$_{urea}$ bond distance of 2.13 Å, which is also in agreement with the experimentally reported value of 2.072 Å. The complex [Mn^{III}H$_3$buea (O)]$^{-2}$ has more symmetrical H-bond cavity with the average hydrogen bond distance of 1.80 Å (see Figure 7), and also the apical nitrogen, manganese and the oxygen lie in the same plane, which shows the linearity of these structures than the [Mn^{II}H$_2$buea(OH)]$^{-2}$ complex.

DFT optimised structure has shown that in [Mn^{IV}H$_3$buea (O)]$^{1-}$ the Mn−O distance is shortened to 1.68 Å in high-spin and 1.66 Å in doublet spin state (see Figure 7). Also, the Mn−N$_{equi}$ bonds are shortened to 1.92 Å to 1.98 Å, indicating a strong interaction of ligand donor atoms with high valent Mn^{IV} species and the geometrical parameters computed are in broad agreement with the earlier study.[26] The N3−Mn−N4, N1−Mn−N3, and N1−Mn−N4 are computed to be 110.4^0, 133.2^0 and 109.3^0, respectively, are consistent with the study, but these angles have deviated from the trigonal symmetry. This distortion in the trigonal plane is due to the Jahn-Teller distortion around the Mn^{IV} metal centre. This is confirmed by optical features having a more intense band at λ$_{max}$ at 635 nm (we reproduced the value computationally and found λ$_{max}$ at 625 nm, see supporting information, Figure S16), and from the EPR spectrum,[26] collected at 4 K has a g values of 5.15, 2.44, and 1.63, which corresponds to S = 3/2 state with an E/D = 0.26, indicating the manganese in +4 oxidation state. From the vibrational features, we obtained a value at 839.4 cm^{-1} corresponds to ν(Mn−O), which is somewhat larger than the experimentally calculated FTIR at 737 cm^{-1}, but it is comparable to other Mn^{IV}=O vibration features for [Mn^{IV}−TMP (O)] (TMP, tetramesitylporphyrin).[26]

On the formation mechanism of Mn−Oxo: Theory vs experiments: Experimentally significant insights are gained on the formation of Mn^{III}=O and Mn^{IV}=O species. Of particular relevance here is the need for H$_2$O to produce Mn^{III}=O species and the additional equivalent of base needed possibly to deprotonate one of the uryl nitrogen atoms. Additionally, the entire reaction completes under Argon atmosphere at room
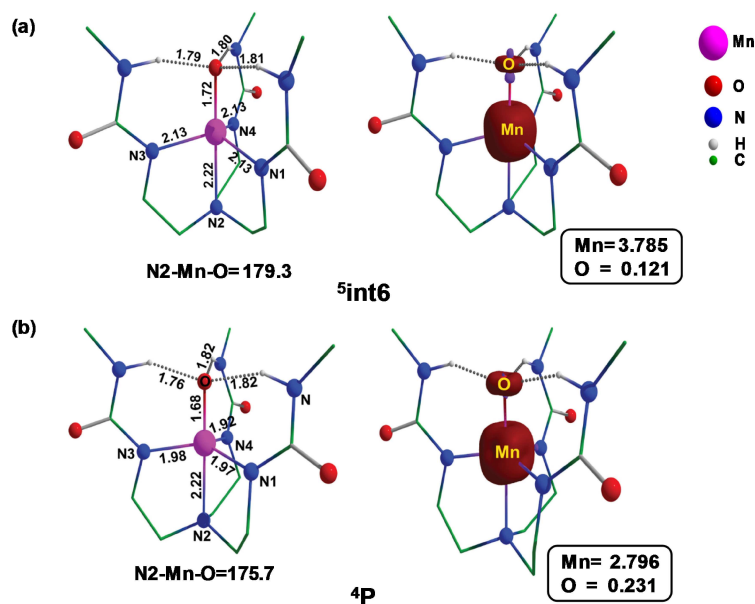

Figure 7. DFT optimized structure of (a) ^{5}int6 with important bonding parameters and its respective spin density plot and (b) ^{4}P with important bonding parameters and its respective spin density plot.

These are not the final page numbers! ↗↗

temperature in a facile fashion. Our mechanism developed suggests that upon O_2 activation, the Mn^{II} precursor yields a rather unusual $[Mn^{II}(O_2^{•-})]$ superoxo species[27] with a significant radical character on the deprotonated uryl nitrogen atom.[31] The generation of this radical character at this site is found to be crucial in dictating various barrier height for the other steps, rationalising the experimental observations that it is mandatory to have an additional equivalent of a base for the generation of Mn–O species. Our attempt to have an overall negative charge at the uryl nitrogen atom was failed, and this suggests that the oxidation state of the superoxo species is unaltered upon O_2 activation. Experimentally bubbling O_2 in the Mn^{II} precursor leads to significant colour change, and the presence of acetate found not to alter the oxidation state of the precursor. While there is no direct experimental evidence for this species, our calculations suggest that formation of such superoxo species is facile and exothermic, suggesting a significant lifetime at lower temperatures.

In the next step, the highly reactive superoxo abstract a hydrogen atom from the DMA solvent leading to $[Mn^{II}(OOH)]$ species. Although there is a significant kinetic barrier for this process at quartet surface (91.6 kJ/mol from sextet surface with an expected MECP), this process is expected to be facile, as from the reactant energies. This is due to the fact that; the overall barrier is still negative as the superoxo species formation is significantly exergonic. The $[Mn^{II}(OOH)]$ thus formed expected to undergo O–O bond cleavage to generate the desired Mn^{III}=O species. However, this species found to strongly form H-bonding interaction with available water molecules before undergoing O–O cleavage. This justifies the need for water in the reaction mixture in the experimental conditions. In the presence of water, the O–O bond cleavage was found to be favourable though there is a significant barrier for the same (179.7 kJ/mol). A significant stabilisation of $[Mn^{II}(OOH)]$ with water leads to an intermediate $[Mn^{II}(OOH_2)]$ which act as a thermodynamic sink to yield desired momentum for the reaction to proceed forward. Interestingly, the O–O cleavage generates a Mn^{III}=O species with a radical centre on the uryl nitrogen atom. Experimentally if wet reagents are employed, the formation of $[Mn^{III}(OH)]$ was favourable, and this perhaps provides indirect evidence that the uryl nitrogen is still deprotonated until the formation Mn^{III}=O and in our case, remains as radical nitrogen until this step. In the ensuing steps, hydrogen atom abstraction from DMA expected to generate $[Mn^{III}(OH)]$ species without much kinetic barrier, and in the next step intramolecular H atom transfer from $[Mn^{III}(OH)]$ to nitrogen N atom leads to formation the final Mn^{III}=O species. The estimated barriers for all the reactions are small, and more importantly from the reactant perspective, all the energetics are negative suggesting a facile formation of this species. The Mn^{III}=O thus formed is very stable with a significant gain in thermodynamic energy and is found to very stable in its S = 2 states as reported in the experiments. In the next step, oxidation of Mn^{III}=O to Mn^{IV}=O is assumed, and this step is computed to be endothermic by 48.9 kJ/mol, and experimentally this is achieved using chemical oxidant such as Cp_2Fe^+.

Additionally, all the structural and spectral parameters computed for the Mn^{III}=O and Mn^{IV}=O species are in agreement with the experiments offering confidence on the proposed mechanism.

4. Conclusions

Herein, we have investigated the various possible pathways for the formation of a mononuclear Mn^{IV}=O species from the Mn^{II} precursor via Mn^{III}=O species, and also we have explored the electronic structure, energies, and properties of all possible intermediates and transition states involved in the mechanism. The following conclusions emerge from this study.

(i) *Oxygen activation*: The Mn^{II} precursor exclusively react with S = 5/2 state and other possible spin-state such as S = 3/2, and S = 1/2 state found not to involve in the reactivity - this is drastically different to known reactivity of the corresponding Fe complexes. Oxygen activation by the $[Mn^{II}H_2buea]^{2-}$ is found to be facile generating a unusual $[Mn^{II}(O_2^{-•})]$ superoxo species with a significant radical character on the deprotonated uryl $N_{α'}$ nitrogen atom.

(ii) *Hyderoperoxo formation*: In the next step, the superoxo species abstract HAT from dimethylacetamide leading to the generation of the $[Mn^{II}(OOH)]$. Despite a fact that in the first step spin states do not play any role, here the spin channels due to the presence of radical character at the $O_2^{•-}$ and $N_{α'}$ nitrogen lead to various spin channels with the lowest barrier estimated on S = 3/2 state arising from spin-up configuration of high-spin Mn^{II} and spin-down on both radicals. While the nature of spin-channels is different here, it is quite clear that these spin-channels offer a significant reduction in the kinetic barrier upholding the important of two-state reactivity concept in such cases.

(iii) *O•••O homolysis:* In the next step O•••O homolysis takes place. Initially, we attempt to model the same using DMA as a proton donor, but the barrier for the same are substantially higher. However, the inclusion of water found to stabilise the transition state significantly. This stabilisation essentially arises from the fact that the transition state is preceded by an intermediate where the –OOH group is in H-bonding interaction with the water leading to elongation of O•••O bond and this facilitate easy cleavage of the bond leading to the formation of Mn^{III}=O species. Experimentally the importance of one equivalent of water in the reaction condition supports the above mechanistic findings. Each step as it proceeds found to be more exergonic than the preceding step easing out the energy penalty arising due to the kinetic barriers. Thus from the reactant perspective, these are overall a barrierless facile process.

(iv) *Formation of Mn^{III}=O species:* A stable Mn^{III}=O species form via a putative Mn^{II}–OH species wherein the solvent plays an important role in providing the protons required.

In this process, the $N_{\alpha'}$ nitrogen gets protonated via an intramolecular H atom transfer leading to $[Mn^{III}H_3buea(O)]^{2-}$ species. Experimentally it is mandatory to have one additional equivalent of a base to generate this species, support our mechanism. Further, the $Mn^{III}{=}O$ species has been experimentally characterised using various spectral methods and our computation reasonably reproduce these numbers offering confidence on the mechanistic findings.

(v) *Formation of $Mn^{IV}{=}O$ species:* Clearly formation of $Mn^{IV}{=}O$ is found to a slightly endothermic and the $Mn^{III}{=}O$ species preceding this species is very stable. This suggests a possible external oxidant that is required to oxidise the Mn atom further as has been observed experimentally.

To this end, using density functional methods, we have explored the mechanism of the formation of putative $Mn^{III}{=}O$ and $Mn^{IV}{=}O$ species using oxygen as an oxidant and several key mechanistic findings arising from this study likely to have a scope in various enzymatic reactions including that of OEC of photosystem II.
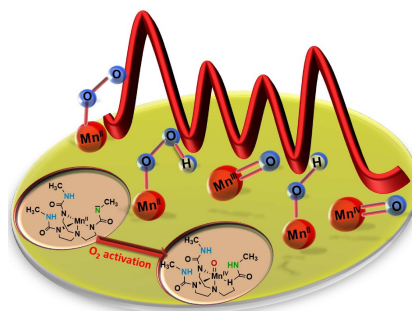
Acknowledgements

References

[1] a) M. M. Abu-Omar, A. Loaiza, N. Hontzeas, *Chem. Rev.* **2005**, *105*, 2227–2252; b) P. R. O. De Montellano, *Cytochrome P450: structure, mechanism, and biochemistry*, 3rd ed.; Kluwer: New York, **2005**; c) C. Krebs, D. Fujimori, C. Walsh, J. Bollinger Jr, *Curr. Opin. Chem. Biol.* **1999**, *9*, 722–731; d) M. T. Green, *Curr. Opin. Chem. Biol.* **2009**, *13*, 84–88; e) P. R. Ortiz de Montellano, *Chem. Rev.* **2009**, *110*, 932–948; f) S. Shaik, W. Lai, H. Chen, Y. Wang, *Acc. Chem. Res.* **2010**, *43*, 1154–1165.

[2] a) J.-Y. Ryu, S.-O. Kim, W.-W. Nam, S.-Y. Heo, J.-H. Kim, *Bull. Korean Chem. Soc.* **2003**, *24*, 1835–1837; b) K. Chen, M. Costas, L. Que Jr, *J. Chem. Soc., Dalton Trans* **2002**, 672–679; c) L. Que Jr, R. Y. Ho, *Chem. Rev.* **1996**, *96*, 2607–2624; d) M. Fontecave, S. Ménage, C. Duboc-Toia, *Coord. Chem. Rev.* **1998**, *178*, 1555–1572; e) J. T. Groves, Y.-Z. Han, in *Cytochrome P450*, Springer, **1995**, pp. 3–48; f) K. Srinivasan, P. Michaud, J. K. Kochi, *J. Am. Chem. Soc.* **1986**, *108*, 2309–2320; g) N. Jin, J. T. Groves, *J. Am. Chem. Soc.* **1999**, *121*, 2923–2924; h) J. T. Groves, J. Lee, S. S. Marla, *J. Am. Chem. Soc.* **1997**, *119*, 6269–6273; i) W. Nam, J. S. Valentine, *J. Am. Chem. Soc.* **1993**, *115*, 1772–1778; j) S. Rana, J. P. Biswas, A. Sen, M. Clémancey, G. Blondin, J.-M. Latour, G. Rajaraman, D. Maiti, *Chem. Sci.* **2018**, *9*, 7843–7858.

[3] a) M. Costas, M. P. Mehn, M. P. Jensen, L. Que, *Chem. Rev.* **2004**, *104*, 939–986; b) W. Nam, *Acc. Chem. Res.* **2007**, *40*, 522–531; c) X. Wu, M. S. Seo, K. M. Davis, Y.-M. Lee, J. Chen, K.-B. Cho, Y. N. Pushkar, W. Nam, *J. Am. Chem. Soc.* **2011**, *133*, 20088–20091; d) A. Borovik, *Chem. Soc. Rev.* **2011**, *40*, 1870–1874; e) A. Gunay, K. H. Theopold, *Chem. Rev.* **2010**, *110*, 1060–1081; f) J. J. Warren, T. A. Tronic, J. M. Mayer, *Chem. Rev.* **2010**, *110*, 6961–7001.

[4] a) D. Kumar, E. Derat, A. M. Khenkin, R. Neumann, S. Shaik, *J. Am. Chem. Soc.* **2005**, *127*, 17712–17718; b) M.-J. Kang, W. J. Song, A.-R. Han, Y. S. Choi, H. G. Jang, W. Nam, *J. Org. Chem.* **2007**, *72*, 6301–6304; c) D. Wang, M. Zhang, P. Bühlmann, L. Que Jr, *J. Am. Chem. Soc.* **2010**, *132*, 7638–7644; d) A. Ansari, A. Kaushik, G. Rajaraman, *J. Am. Chem. Soc.* **2013**, *135*, 4235–4249; e) P. Comba, G. Rajaraman, *Inorg. Chem.* **2008**, *47*, 78–93; f) J. C. Schöneboom, S. Cohen, H. Lin, S. Shaik, W. Thiel, *J. Am. Chem. Soc.* **2004**, *126*, 4017–4034; g) D. Kumar, S. P. de Visser, S. Shaik, *J. Am. Chem. Soc.* **2004**, *126*, 3368–3368; h) D. Kumar, S. P. de Visser, S. Shaik, *J. Am. Chem. Soc.* **2003**, *125*, 13024–13025; i) M. Filatov, N. Harris, S. Shaik, *Angew. Chem. Int. Ed.* **1999**, *38*, 3510–3512; *Angew. Chem.* **1999**, *111*, 3730–3733; j) C. V. Sastri, J. Lee, K. Oh, Y. J. Lee, J. Lee, T. A. Jackson, K. Ray, H. Hirao, W. Shin, J. A. Halfen, *Proc. Natl. Acad. Sci.* **2007**, *104*, 19181–19186; k) S. P. de Visser, K. Oh, A.-R. Han, W. Nam, *Inorg. Chem.* **2007**, *46*, 4632–4641; l) M. R. Bukowski, P. Comba, A. Lienke, C. Limberg, C. Lopez de Laorden, R. Mas-Ballesté, M. Merz, L. Que Jr, *Angew. Chem. Int. Ed.* **2006**, *45*, 3446–3449; *Angew. Chem.* **2006**, *118*, 3524–3528.

[5] a) V. K. Yachandra, K. Sauer, M. P. Klein, *Chem. Rev.* **1996**, *96*, 2927–2950; b) C. Tommos, J. McCracken, S. Styring, G. T. Babcock, *J. Am. Chem. Soc.* **1998**, *120*, 10441–10452; c) V. L. Pecoraro, M. J. Baldwin, M. T. Caudle, W.-Y. Hsieh, N. A. Law, *Pure Appl. Chem.* **1998**, *70*, 925–929; d) X.-S. Tang, D. W. Randall, D. A. Force, B. A. Diner, R. D. Britt, *J. Am. Chem. Soc.* **1996**, *118*, 7638–7639; e) M. L. Gilchrist, J. A. Ball, D. W. Randall, R. D. Britt, *Proc. Natl. Acad. Sci.* **1995**, *92*, 9545–9549.

[6] R. J. Nick, G. B. Ray, K. M. Fish, T. G. Spiro, J. T. Groves, *J. Am. Chem. Soc.* **1991**, *113*, 1838–1840.

[7] H. Komatsuzaki, N. Sakamoto, M. Satoh, S. Hikichi, M. Akita, Y. Moro-oka, *Inorg. Chem.* **1998**, *37*, 6554–6555.

[8] Z. Shirin, B. S. Hammes, V. G. Young, A. S. Borovik, *J. Am. Chem. Soc.* **2000**, *122*, 1836–1837.

[9] R. Gupta, A. Borovik, *J. Am. Chem. Soc.* **2003**, *125*, 13234–13242.

[10] C. E. MacBeth, R. Gupta, K. R. Mitchell-Koch, V. G. Young Jr, G. H. Lushington, W. H. Thompson, M. P. Hendrich, A. Borovik, *J. Am. Chem. Soc.* **2004**, *126*, 2556–2567.

[11] T. H. Parsell, M.-Y. Yang, A. Borovik, *J. Am. Chem. Soc.* **2009**, *131*, 2762–2763.

[12] a) W. Zhang, J. L. Loebach, S. R. Wilson, E. N. Jacobsen, *J. Am. Chem. Soc.* **1990**, *112*, 2801–2803; b) M. Palucki, N. S. Finney, P. J. Pospisil, M. L. Güler, T. Ishida, E. N. Jacobsen, *J. Am. Chem. Soc.* **1998**, *120*, 948–954; c) J. T. Groves, *J. Porphyrins Phthalocyanines* **2000**, *4*, 350–352.

[13] a) A. Borovik, *Acc. Chem. Res.* **2005**, *38*, 54–61; b) F. Bordwell, H. E. Fried, D. L. Hughes, T. Y. Lynch, A. Satish, Y. E. Whang, *J. Org. Chem.* **1990**, *55*, 3330–3336; c) B. S. Hammes, V. G. Young, Jr., A. S. Borovik, *Angew. Chem. Int. Ed.* **1999**, *38*, 666–669; *Angew. Chem.* **1999**, *111*, 741–743; d) D. C. Lacy, J. Mukherjee, R. L. Lucas, V. W. Day, A. Borovik, *Polyhedron* **2013**, *52*, 261–267; e) C. Nozaki, C. G. Lugmair, A. T. Bell, T. D. Tilley, *J. Am. Chem. Soc.* **2002**, *124*, 13194–13203.

[14] M. Jaccob, A. Ansari, B. Pandey, G. Rajaraman, *Dalton Trans.* **2013**, *42*, 16518–16526.

[15] a) S. P. de Visser, Y. M. Lee, W. Nam, *Eur. J. Inorg. Chem.* **2008**, *2008*, 1027–1030; b) H. Hirao, L. Que Jr, W. Nam, S. Shaik,

Chem. Eur. J. **2008**, *14*, 1740–1756; c) S. P. de Visser, M. G. Quesne, B. Martin, P. Comba, U. Ryde, *Chem. Commun.* **2014**, *50*, 262–282; d) A. Ansari, G. Rajaraman, *Dataset Papers in Science* **2014**, *2014*.

[16] M. Frisch, G. Trucks, H. Schlegel, G. Scuseria, M. Robb, J. Cheeseman, G. Scalmani, V. Barone, B. Mennucci, G. Petersson, *Gaussian 09 Revision A* **2009**, *1*.

[17] A. D. Becke, *J. Chem. Phys.* **1997**, *107*, 8554–8560.

[18] a) E. v. Lenthe, E.-J. Baerends, J. G. Snijders, *J. Chem. Phys.* **1993**, *99*, 4597–4610; b) C. van Wüllen, *J. Chem. Phys.* **1998**, *109*, 392–399.

[19] F. Neese, *Wiley Interdiscip. Rev.: Comput. Mol. Sci.* **2012**, *2*, 73–78.

[20] F. Neese, *J. Chem. Phys.* **2007**, *127*, 164112.

[21] R. L. Shook, W. A. Gunderson, J. Greaves, J. W. Ziller, M. P. Hendrich, A. S. Borovik, *J. Am. Chem. Soc.* **2008**, *130*, 8888–8889.

[22] a) C. Duboc, D. Ganyushin, K. Sivalingam, M.-N. Collomb, F. Neese, *J. Phys. Chem. A.* **2010**, *114*, 10750–10758; b) F. Neese, *J. Am. Chem. Soc.* **2006**, *128*, 10213–10222.

[23] a) F. Ogliaro, S. P. de Visser, S. Cohen, P. K. Sharma, S. Shaik, *J. Am. Chem. Soc.* **2002**, *124*, 2806–2817; b) J. Cho, S. Jeon, S. A. Wilson, L. V. Liu, E. A. Kang, J. J. Braymer, M. H. Lim, B. Hedman, K. O. Hodgson, J. S. Valentine, *Nature* **2011**, *478*, 502; c) M. Martinho, F. Banse, J. Sainton, C. Philouze, R. Guillot, G.

Blain, P. Dorlet, S. Lecomte, J.-J. Girerd, *Inorg. Chem.* **2007**, *46*, 1709–1717.

[24] R. S. Czernuszewicz, Y. O. Su, M. K. Stern, K. A. Macor, D. Kim, J. T. Groves, T. G. Spiro, *J. Am. Chem. Soc.* **1988**, *110*, 4158–4165.

[25] T. J. Collins, R. D. Powell, C. Slebodnick, E. S. Uffelman, *J. Am. Chem. Soc.* **1990**, *112*, 899–901.

[26] T. H. Parsell, R. K. Behan, M. T. Green, M. P. Hendrich, A. Borovik, *J. Am. Chem. Soc.* **2006**, *128*, 8728–8729.

[27] N. Schuth, S. Mebs, D. Huwald, P. Wrzolek, M. Schwalbe, A. Hemschemeier, M. Haumann, *Proc. Natl. Acad. Sci.* **2017**, *114*, 8556–8561.

[28] B. Mennucci, *Wiley Interdiscip. Rev.: Comput. Mol. Sci.* **2012**, *2*, 386–404.

[29] F. Neese, *Wiley Interdiscip. Rev.: Comput. Mol. Sci.* **2011**, *2*, 73–78.

[30] D. M. Kurtz Jr, *Chem. Rev.* **1990**, *90*, 585–606.

[31] J. Rajpurohit, P. Shukla, P. Kumar, C. Das, S. Vaidya, M. Sundararajan, M. Shanmugam, M. Shanmugam, *Inorg. Chem.* **2019**, *58*, 6257–6267.

FULL PAPER

How high-valent Mn–oxo species are generated in bio-mimic environment? Our study unveils the mechanistic intricacy involved in generating the species, which has high relevance for the OEC.

A. Sen, N. Vyas*, B. Pandey, M. Jaccob, G. Rajaraman*

Mechanistic Insights on the Formation of high-valent $Mn^{III/IV}=O$ Species Using Oxygen as Oxidant: A Theoretical Perspective